EUROFUSION WPJET1-PR(16) 14698

C Guillemaut et al.

Evidence for enhanced main chamber wall plasma loads in JET ITER-like Wall at high radiated fraction

Preprint of Paper to be submitted for publication in
22nd International Conference on Plasma Surface Interactions
in Controlled Fusion Devices (22nd PSI)

This work has been carried out within the framework of the EUROfusion Consortium and has received funding from the Euratom research and training programme 2014-2018 under grant agreement No 633053. The views and opinions expressed herein do not necessarily reflect those of the European Commission.

Main chamber wall plasma loads in JET-ITER-like Wall at high radiated fraction

C. Guillemaut[a,b], P. Drewelow[c], G.F. Matthews[d], A.S. Kukushkin[e,f], R.A. Pitts[g], P. Abreu[b], S. Brezinsek[h], M. Brix[d], P. Carman[d], R. Coelho[b], S. Devaux[j], J. Flanagan[d], C. Giroud[d], D. Harting[d], C.G. Lowry[j], C.F. Maggi[d], F. Militello[d], C. Perez Von Thun[h], E.R. Solano[k], A. Widdowson[d], S. Wiesen[h], M. Wischmeier[l], D. Wood[d], and JET contributors[*]

[a] *EUROfusion Consortium, JET, Culham Science Centre, Abingdon, OX14 3DB, UK*

[b] *Instituto de Plasmas e Fusao Nuclear, Instituto Superior Tecnico, Universidade Lisboa, Portugal*

[c] *Max-Planck-Institut fur Plasmaphysik, Teilinsitut Greifswald, D-17491 Greifswald, Germany*

[d] *CCFE, Culham Science Centre, Abingdon OX14 3DB, UK*

[e] *Kurshatov Institute, Akademika Kurchatova pl., Moscow, 123182, Russia*

[f] *NRNU MEPHi, Kashirskije sh. 31, Moscow, 115406, Russia*

[g] *ITER Organization, Route de Vinon CS 90 046, 13067 Saint-Paul-Lez-Durance, France*

[h] *Forschungszentrum Jülich GmbH, Institut für Energie- und Klimaforschung – Plasmaphysik, 52425 Jülich, Germany*

[i] *Institut Jean Lamour, UMR7198 CNRS—Université de Lorraine, F-54506 Vandoeuvre-les-Nancy Cedex, France*

[j] *European Commision, B-1049 Brussels, Belgium*

[k] *Laboratorio Nacional de Fusión,CIEMAT, 28040 Madrid, Spain*

[l] *Max-Planck-Institut fur Plasmaphysik, 85748 Garching bei Munchen, Germany*

Email: christophe.guillemaut@ukaea.uk

Abstract

Future tokamak reactors of conventional design will require high levels of exhaust power dissipation (more than 90% of the input power) if power densities at the divertor targets are to remain compatible with active cooling. Impurity seeded H-mode discharges in JET-ITER-like Wall (ILW) have reached a maximum radiative fraction (F_{rad}) of ~ 75%. Divertor Langmuir probe (LP) measurements in these discharges indicate, however, that less than ~ 3% of the thermal plasma power reaches the targets, suggesting a missing channel for power loss. This paper presents experimental evidence from LP for enhanced cross-field particle fluxes on the main chamber walls at high F_{rad}. In H-mode nitrogen seeded discharges with F_{rad} increasing from ~ 30 % to up to ~ 75 %, the main chamber wall particle fluence rises by a factor ~ 3 while the divertor plasma fluence drops by one order of magnitude. Contribution of main chamber wall particle losses to detachment, as suggested by

EDGE2D-EIRENE modelling, is not sufficient to explain the magnitude of the observed divertor fluence reduction. An intermediate detached case obtained at F_{rad} ~ 60 % with neon seeding is also presented. Heat loads have been obtained using the main chamber wall thermocouples. Comparison between thermocouple and bolometry measurements shows that the fraction of input power transported to the main chamber wall remains below ~ 5% whether the divertor is attached or detached. Main chamber sputtering of beryllium by deuterium is reduced in detached conditions only on the low field side. If the fraction of power exhaust dissipated to the main chamber wall by cross-field transport in future reactors is similar to JET-ILW levels, it should not be an issue.

[*] *See the Appendix of F. Romanelli et al., Proceedings of the 25th IAEA Fusion Energy Conference 2014, Saint Petersburg, Russia*

1. Introduction

Future tokamak reactors of conventional design will have to dissipate more than 90% of the exhaust power to keep the heat flux densities at the divertor targets at feasible levels for active cooling [1]. The JET-ITER-like Wall (ILW) [2] comprises a tungsten (W) divertor and beryllium (Be) main chamber wall thus matching the material configuration planned for ITER. Since W and Be are very poor radiators in the Scrape-Off Layer (SOL), the seeding of impurities like nitrogen (N), neon (Ne) or argon (Ar) can be used to dissipate significant amounts of power radiatively. High power, N and Ne seeded H-mode discharges in JET-ILW have reached a maximum radiative fraction (F_{rad}) of ~ 75% and ~ 60%, respectively [3], see Fig.1. However, the fraction of thermal plasma power reaching the targets (see Table 1) obtained by surface integration of power density profiles (Fig. 2) from divertor Langmuir probe (LP) measurements (see positions in Fig. 3) is insufficient, suggesting a missing channel for power loss.

According to 2D fluid-neutral modelling with EDGE2D-EIRENE [4-6], divertor detachment is due to a combination of three particle losses: volume recombination, molecular activated recombination and cross-field transport [7]. Therefore some exhaust power may be dissipated on the main chamber wall by filamentary cross-field transport. The purpose of this paper is to study the relation between main

chamber wall plasma loads and divertor detachment. The deeply detached maximum F_{rad} JET-ILW discharge #85425 with N seeding offers good conditions for such study. Discharge #85441 using Ne seeding provides intermediate detached conditions and #84884 is the reference unseeded attached discharge. This series of experiments in JET-ILW used a low triangularity with inner and outer vertical target divertor configuration. The plasmas have been achieved in a toroidal magnetic field of 2.6 T with a plasma current of 2.5 MA. During impurity seeding, the heating power was around ~ 18 MW and was provided by neutral beam injection (NBI) only.

As shown in Fig. 3, two of the JET-ILW inner and outer wall guard limiters are equipped with poloidal arrays of respectively 16 and 20 LP which can be used to provide an indication of the wall ion flux, even during diverted discharges when the plasma-wall distances are large. Particle flux densities (J_{sat}) on the individual limiter LP during diverted operations are too small to allow electron temperature measurements using a voltage sweep so heat loads have been obtained using the main chamber wall thermocouples placed in the same limiters as the LP. Although wide angle infrared thermography is available for the main chamber wall, it could not be used for this purpose here because of the level of the signal is too low and cannot be distinguished from background noise. Ratio of heat load by particle flux density allows estimation of ion impact energies and Be sputtering by D on main chamber wall.

In this paper, the evolution of limiter LP particle fluence measurements with detachment is presented in Section 2. In Section 3, correlation of limiter particle flux variations with changes in edge density profiles and filament activity is discussed. In Section 4, plasma heat loads on main chamber wall are estimated by comparing thermocouple with bolometry measurements. Finally, Be sputtering by D on the main chamber wall is discussed in Section 5.

2. Particle fluence on main chamber wall limiters during radiative scenarios

Particle fluence has been calculated by time integration of LP J_{sat} measurements on inner and outer limiters over the ~ 10 s NBI flat top in discharges #85425, #85441 and #84884. For clarity and because of the strength of the signals, the poloidal profiles shown in Fig. 4 have been obtained from the LP closest to the center of the limiters and on the side exposed to the plasma (red dots in Fig. 3). These values

have been plotted against the s coordinate following the main chamber poloidal contour in anti-clockwise direction, starting at 0 at the edge of the inner divertor and ending at the lower edge of the inner limiter at around 10 m. Since most of the inner limiter LP were not working in #84884, this data has been completed with measurements made in the equivalent unseeded attached discharge #83487.

In Fig. 4, the particle fluence on the outer limiter increases from the range ~ 1.8 – 2.8 x 10^{22} m^{-2} in attached conditions to ~ 5 – 7.5 x 10^{22} m^{-2} with Ne seeding and up to ~ 8 – 12 x 10^{22} m^{-2} with deeply detached N seeded divertor. On the inner limiter, the increase of particle fluence goes from the range ~ 2.3 – 3 x 10^{22} m^{-2} in attached conditions to ~ 6 – 8 x 10^{22} m^{-2} with Ne seeding and with N seeding. In these discharges, the separatrix-wall distance ranges from 6 to 14 cm outboard and from 15 to 18 cm inboard.

The total amount of particles collected on the limiters during the NBI flat top is calculated by multiplying the fluence from each LP by their associated limiter area (see magenta zones in Fig. 3) and by the number of limiters. The counts for the different regions of the plasma chamber shown in Table 2 are obtained considering that there are 11 equivalent outer limiters and 10 inner limiters. In Ne seeded detached conditions, the total number of particles collected on the main chamber wall is increased by a factor ~ 2 compared to attached conditions while it is divided by ~ 2 in the divertor. In N seeded detached conditions, the wall particle count increases by a factor ~ 3 compared to the attached case while it is divided by ~ 10 in the divertor. Overall, ~ 4 % of the particles are transported to the main chamber wall limiters in attached conditions, ~ 18 % in Ne detached conditions and ~ 52 % in N detached conditions.

The idea that particle losses by cross-field transport contribute to some extent to divertor detachment, is suggested by EDGE2D-EIRENE modelling [7,8]. However, between unseeded attached conditions and fully detached N seeded conditions, the divertor loses 54.4 x 10^{23} particles while the wall only gains 4.7 x 10^{23} particles which indicates that particle losses on the main chamber wall due to cross-field transport remains a small contribution to the detachment process. As discussed in [7,9], significant volume effects such as volume recombination and molecular activated recombinations are likely to be involved to explain the enormous particle loss in the detached divertor of discharge #85425.

3. Correlation of limiter particle flux with edge density profiles and filaments

In previous L-mode studies, enhanced particle loads on the main chamber wall in detached conditions were associated with broadening of the electron density (n_e) profile and enhanced filamentary cross-field transport, see [10-13]. In the experiments studied here, the far SOL midplane density was accessible through Li-Beam measurements (see Fig. 3) only in the unseeded attached case and the N seeded detached case. It is clear in Fig. 5 that n_e at the very edge of the profile is nearly a factor ~ 2 higher when the divertor is detached

A particular feature of high F_{rad} experiments is the disappearance of Type I ELMs when F_{rad} > 60 – 65 % with Ne and N seeding while the energy confinement time remains around ~ 300 ms as in unseeded attached conditions. Consistently with previous Section results, comparison of J_{sat} measurements from limiter LP 11 (see Fig. 3d for position) and the divertor LP shows opposite behaviors with an increase of particle flux on the main chamber wall (Fig. 6a) while the divertor particle flux is strongly reduced during detachment (Fig. 6b and c). Inspection of high time resolution limiter LP 11 J_{sat} measurements reveals some particle bursts (Fig. 6a) which are only present in Ne and N seeded detached conditions when Type I ELMs have vanished. These structures can be observed on all limiter LP and are due to enhanced filamentary cross-field transport. They have a frequency of the order of ~ 1 kHz which may be related to Type III ELMs activity.

The transport of particles to the main chamber wall generates a plasma heat load which adds up to the radiative heat load. Both contributions are estimated in the next Section.

4. Plasma heat loads on main chamber wall during radiative scenarios

Particle fluxes on individual limiter probes during diverted operation are too small to allow electron temperature measurements using a voltage sweep so heat loads have been obtained using the thermocouples embedded in some of the tiles of the main chamber wall, see Fig. 3b. They measure bulk tile temperatures in degree Celsius. Therefore, the energy Q_{tile} (in J) accumulated in a given tile during a discharge can be calculated with the temperature variation ΔT (in Celsius or K) between the beginning and the end of the experiment, the heat capacity C_p (in J.kg^{-}

^{1}.K^{-1}) of the tile material and its mass m (in kg) as follows:

$$Q_{tile} = mC_p\Delta T \ . \qquad (1)$$

The main chamber tiles considered here are made with bulk Be with C_p ~ 2390 J.Kg^{-1}.K^{-1} in the range 100 – 200 degrees C of wall temperatures of JET-ILW. Q_{tile} given by the thermocouples cumulates the radiative, charge exchange (CX) and the plasma heating contributions.

An energy density in J.m^{-2} can also be obtained by dividing Q_{tile} from (1) by the area of the tile surface exposed to the plasma flux and radiation. Energy density poloidal profiles from thermocouples are convenient to compare with radiative energy densities deduced from bolometric tomographic reconstructions (Fig. 7a) to estimate the thermal power transported to the main chamber wall. Although the main chamber wall poloidal profile of radiative energy density on Fig. 7b is axisymmetric, the profile of total energy density from the thermocouples exists only on limiters. According to [14], only the radiative contribution should remain in between limiters.

When the radiative contribution is subtracted from the total energy density profile on limiters, the plasma contribution is obtained in Fig. 8 for the three cases considered here. Surface integration of Fig. 8 profiles give ~ 9 MJ, ~ 8.5 MJ and 8 MJ in unseeded, Ne seeded and N seeded conditions respectively. Since the limiter phase contribution to the wall heat load is of the order of ~ 2 MJ, not more than ~ 7 MJ are transported by the plasma to the main chamber wall during the diverted phase. The total input heat during the NBI flat top is around ~ 180 MJ in these experiments thus, only ~ 4 % of it reaches the main chamber wall through the plasma whether the divertor is attached or detached. The peak power density is reached at the inner and outer midplanes and does not exceed ~ 0.1 MW.m^{-2}. If this contribution remains at the same order of magnitude in a reactor, it should not be an issue for the main chamber wall.

5. Changes in main chamber wall sputtering with divertor detachment

On a given limiter tile surface of area A_{tile} (in m^2) exposed to the plasma, the particle

fluence J (in m^{-2}) is linked to Q_{tile} as follows:

$$\frac{Q_{tile}}{A_{tile}} = \gamma T J e \,, \tag{2}$$

with the heat transmission coefficient γ ~ 7 [15] and the electron and ion temperature T_e and T_i (in eV) respectively such as $T \sim T_e \sim T_i$. The ion impact energy E_i (in eV) on the limiters can be deduced as follows:

$$E_i = \gamma_i T \,, \tag{3}$$

with the ion heat transmission coefficient γ_i ~ 2.5 [15]. Therefore, it is possible to use J and Q_{tile} measurements to deduce E_i where limiter probes and thermocouples are physically close enough. The main chamber wall E_i poloidal profile in Fig. 9a is obtained by using the LP on the exposed side (in red in Fig. 3) closest to the limiter tile center and the associated thermocouples.

On the outer limiter, E_i goes up to ~ 100 eV at the midplane in unseeded conditions and falls down to an average of ~ 20 eV and then ~ 10 eV with Ne seeding an N seeding respectively. On the inner limiter E_i reaches nearly ~ 120 eV at the midplane in attached conditions and drops to the range ~ 30 – 50 eV when detachment is obtained with Ne or N. These calculated E_i give access to the Be sputtering yields from [16] plotted in Fig. 9b and allow an estimate of the main chamber limiter Be source in the discharges studied here. Be is dominantly sputtered by D and the source for the 11 outer and 10 inner guard wall limiters have been calculated in Table 3 for the different divertor conditions. Although Ne and N ions are heavier and carry multiple charges, there abundance in the plasma is of the order of ~ 1 % which reduce their contribution to Be sputtering by an order of magnitude compared to D.

It is clear in Table 3 that detachment strongly reduces Be sputtering on the outer limiters while the effect is rather small on the inner limiters because of the weaker E_i reduction along with the increase of particle flux. This is consistent with Be deposition observed on the upper inner divertor tiles in JET-ILW [17-20] and the stronger Be erosion observed on the inner limiters [21]. In each of the discharges

studied here, the mass of Be sputtered by D from the inner limiters during the NBI flat top is of the order of ~ 20 mg. According to [17], ~ 40 g of Be in total have been accumulated on the upper inner divertor tiles over the ~ 3000 discharges of the first JET-ILW campaign which represents an average of ~ 13 mg per discharge. Although this initial campaign mixed many different plasma configurations and input powers, it appears that Be sputtered from inner limiters by direct plasma-wall interaction during divertor phases may contribute significantly to the deposition observed on the inner divertor tiles. Thorough examination of guard wall limiters Be sputtering source with the present method compared to spectroscopy measurements and post-mortem tile analysis should be the object of further studies.

6. Conclusions

Future tokamak reactors of conventional design will have to dissipate more than 90% of the exhaust power to keep the heat flux densities at the divertor targets at feasible levels for active cooling [1]. High power, N and Ne seeded H-mode discharges in JET-ILW have reached a maximum radiative fraction (F_{rad}) of ~ 75% and ~ 60% respectively [3]. Since the fraction of thermal plasma power reaching the targets is insufficient to retrieve the full amount of input power, one or several dissipation channels may be missing. Some exhaust power may be dissipated on the main chamber wall by cross-field filamentary transport which could be an issue in the context of a reactor because of strong restrictions on first wall power loads. Strongly detached high F_{rad} H-mode JET-ILW discharges have been used to study the relation between main chamber wall plasma loads and divertor detachment.

Particle fluence on the main chamber wall measured by limiter LP increases significantly with the level of divertor detachment. However, the amount of particle redirected to the main chamber wall corresponds to less than 10 % of the amount missing in the fully detached divertor. Therefore, other stronger particle sinks must be involved to explain the magnitude of the particle fluence reduction observed by divertor LP during detachment. As suggested by EDGE2D-EIRENE modelling [7], recombination processes may be the dominant contributors.

Main chamber power loads associated with cross-field transport have been estimated by thermocouples and bolometry measurements and should not represent more than 5 % of the input power. If this fraction is similar in future

reactors it should not be an issue for the main chamber wall.

Particle fluence and power load measurements have been used to calculate the ion impact energy on the inner and outer guard wall limiters and estimate the Be sputtering source depending on the level of divertor detachment. Because of the small concentration of N or Ne, Be is dominantly sputtered by D on the limiters. It appears that detachment with impurity seeding strongly reduces the sputtering on the outer limiters but not on the inner limiters. This is consistent with Be deposition observed on the upper inner divertor tiles in JET-ILW [17-20] and the stronger Be erosion observed on the inner limiters [21]. This topic should be the object of further studies.

Acknowledgments

This work has been carried out within the framework of the EUROfusion Consortium and has received funding from the Euratom research. IST activities also received financial support from “Fundação para a Ciência e Tecnologia” through project UID/FIS/50010/2013. The views and opinions expressed herein do not necessarily reflect those of the European Commission.

References

[1] G. Federici et al., Fusion Engineering and Design **89** (2014) 882–889
[2] G.F. Matthews et al. 2011 Phys. Scr. **T145** 014001
[3] M. Wischmeier et al., Journal of Nuclear Materials **463** (2015) 22–29
[4] R. Simonini et al., Contrib. Plasma Phys. 34 (1994) 368
[5] D. Reiter et al., J. Nucl. Mater. 196-198 (1992) 80
[6] S. Wiesen et al, ITC project report (2006),
http://www.eirene.de/e2deir_report_30jun06.pdf
[7] C. Guillemaut et al., Nucl. Fusion **54** (2014) 093012
[8] S. Wiesen et al., Journal of Nuclear Materials **415** (2011) 535-539
[9] S.I. Krasheninnikov et al., Phys. Plasmas **4**, No. 5, 1638- 1346, May 1997
[10] N. Asakura et al., Journal of Nuclear Materials 241, **559-563** (1997)
[11] M.V. Umansky et al., Phys. Plasmas **5**, 3373 (1998)
[12] B. LaBombard et al., Phys. Plasmas **8**, 2107 (2001)

[13] C. Carralero et al., Journal of Nuclear Materials **463** (2015) 123–127
[14] G.F. Matthews et al., PSI 2016
[15] P.C. Stangeby 2000 The Plasma Boundary of Magnetic Fusion Devices (New York: Taylor and Francis)
[16] W. Eckstein et al. 2002 Calculated sputtering, reflection and range values IPP Report IPP 9/132 (Garching: Max-Planck-Institut für Plasmaphysik)
[17] A. Baron-Wiechec et al., Journal of Nuclear Materials **463** (2015) 157–161
[18] K. Heinola et al., Journal of Nuclear Materials **463** (2015) 961–965
[19] A. Widdowson et al., PSI 2016
[20] N. Catarino et al., PSI 2016
[21] S. Brezinsek et al., Nucl. Fusion **55** (2015) 063021

Figure captions:

Fig. 1 From top to bottom: F_{rad} time traces; Ne and N seeding rates time trace.

Fig. 2 From left to right: inner divertor target surface power density profile; same for outer target.

Fig. 3 (a) Position of divertor LP and thermocouples, (b) same as (a) for main chamber, (c) inner guard wall limiter with exposed (red dots) and shadowed (blue dots) LP with associated area (magenta) and (d) same as (c) for outer guard wall limiter.

Fig. 4 Particle fluence poloidal profiles.

Fig. 5 Midplane electron density profile from Li-beam measurements.

Fig. 6 (a) Jsat time trace from limiter LP 11, (b) inner divertor target Jsat profile and (c) same as (b) for outer target.

Fig. 7 (a) Bolometry lines of sight and (b) poloidal profiles of radiative and total energy density along main chamber wall limiters.

Fig. 8 Plasma contribution to energy density poloidal profile along main chamber wall limiters.

Fig. 9 (a) Ei poloidal profiles along inner and outer guard wall limiters and (b) Be sputtering yields from [16].

Table caption:

Table 1 Distribution of exhaust power depending on divertor conditions

Table 2 Distribution of exhaust particles depending on divertor conditions

Table 3 Distribution of Be sputtering due to D depending on divertor conditions

	Unseeded	Ne seeded	N seeded
F_{rad}	30 %	60 %	75 %
F_{div}	49 %	13 %	3 %
Missing fraction	21 %	27 %	22 %

Table 1

	Unseeded	Ne seeded	N seeded
Outer wall	1.77×10^{23}	4.1×10^{23}	5.5×10^{23}
Inner wall	0.85×10^{23}	2×10^{23}	1.8×10^{23}
Divertor	61×10^{23}	27×10^{23}	6.6×10^{23}

Table 2

	Unseeded	Ne seeded	N seeded
Outer wall	2.2×10^{21}	9.9×10^{20}	2.1×10^{20}
Inner wall	1.7×10^{21}	1.1×10^{21}	1.1×10^{21}

Table 3

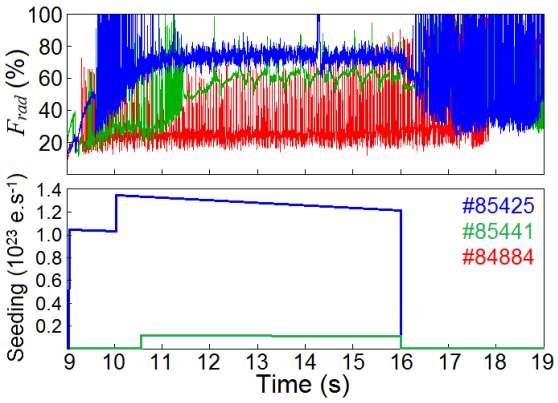
100
80
60
40
20
F_{rad} (%)
1.4
1.2
1.0
0.8
0.6
0.4
0.2
Seeding (10^{23} e.s^{-1})
#85425
#85441
#84884
9
10
11
12
13
14
15
16
17
18
19
Time (s)

Figure 1

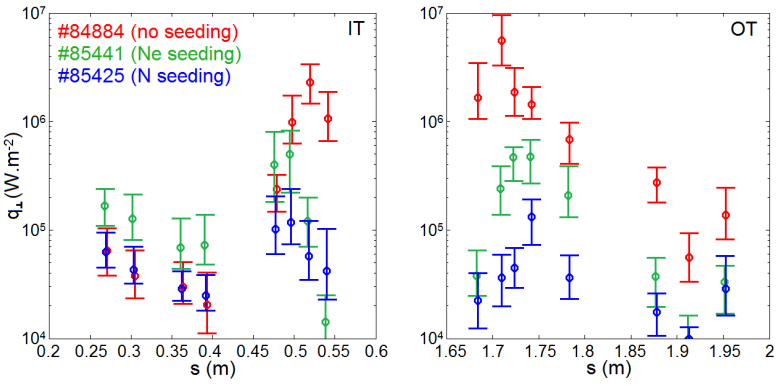
#84884 (no seeding)
#85441 (Ne seeding)
#85425 (N seeding)
IT
OT
$q_\perp$ (W.m^{-2})
s (m)
s (m)

Figure 2

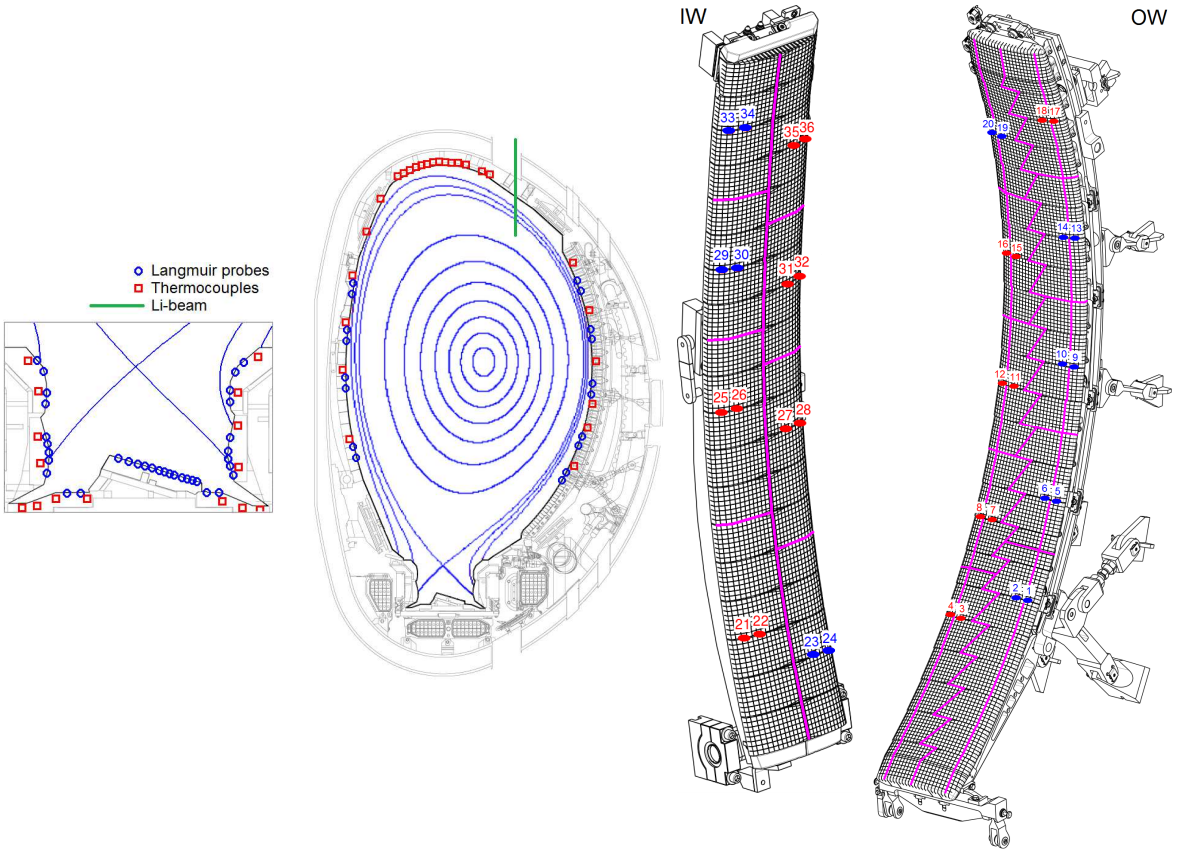

Figure 3

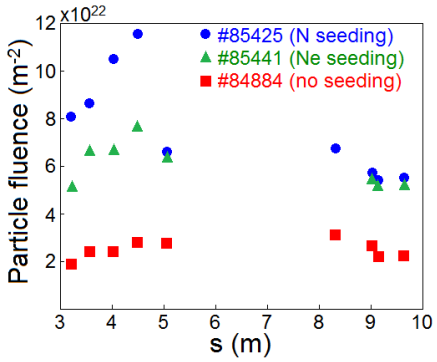
x10^22
12
10
8
6
4
2
Particle fluence (m^-2)
3
4
5
6
7
8
9
10
s (m)
#85425 (N seeding)
#85441 (Ne seeding)
#84884 (no seeding)

Figure 4

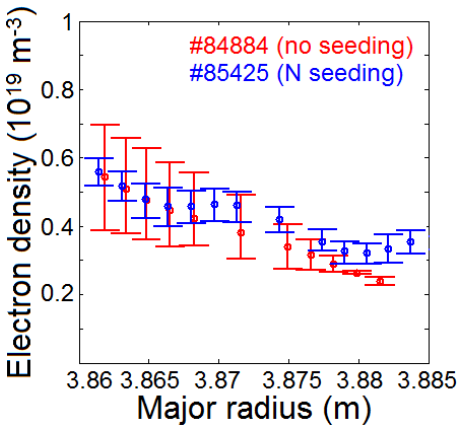
#84884 (no seeding)
#85425 (N seeding)
Electron density (10^{19} m^{-3})
1
0.8
0.6
0.4
0.2
3.86
3.865
3.87
3.875
3.88
3.885
Major radius (m)

Figure 5

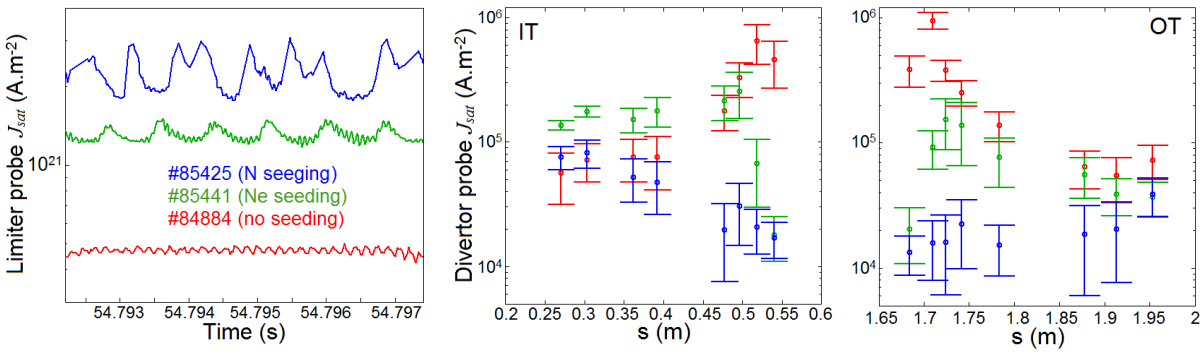
Limiter probe J_{sat} (A.m^{-2})
10^{21}
#85425 (N seeging)
#85441 (Ne seeding)
#84884 (no seeding)
54.793 54.794 54.795 54.796 54.797
Time (s)
Divertor probe J_{sat} (A.m^{-2})
IT
10^6
10^5
10^4
0.2 0.25 0.3 0.35 0.4 0.45 0.5 0.55 0.6
s (m)
OT
10^6
10^5
10^4
1.65 1.7 1.75 1.8 1.85 1.9 1.95 2
s (m)

Figure 6

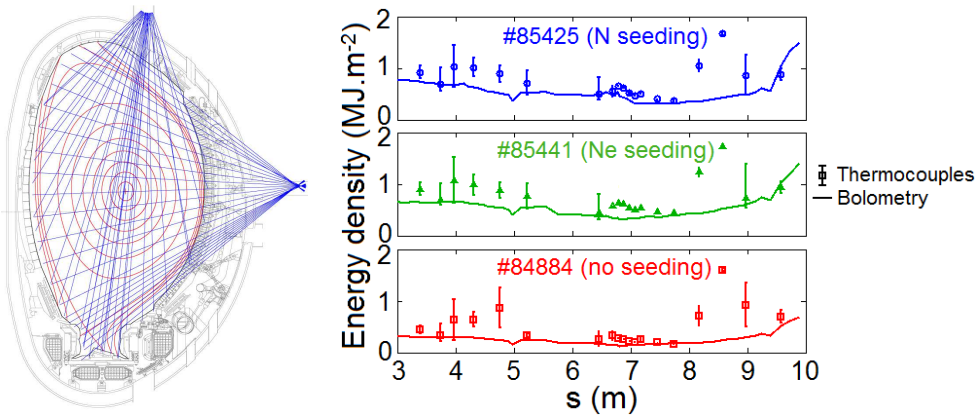
#85425 (N seeding)
#85441 (Ne seeding)
#84884 (no seeding)
Energy density (MJ.m-2)
s (m)
Thermocouples
Bolometry

Figure 7

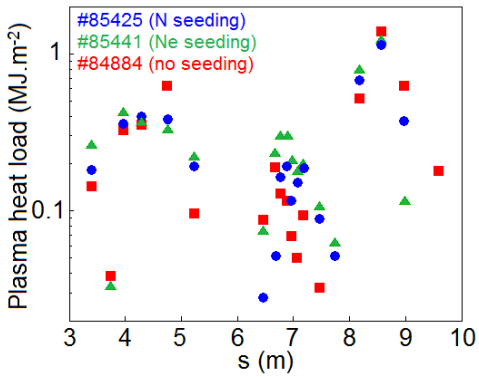
#85425 (N seeding)
#85441 (Ne seeding)
#84884 (no seeding)
Plasma heat load (MJ.m-2)
1
0.1
3
4
5
6
7
8
9
10
s (m)

Figure 8

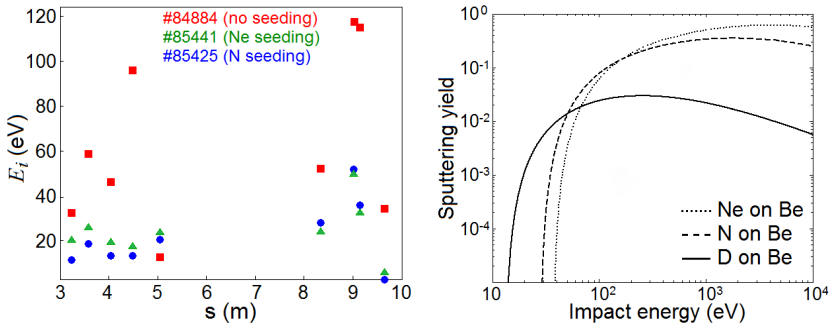
#84884 (no seeding)
#85441 (Ne seeding)
#85425 (N seeding)
E_i (eV)
s (m)
Sputtering yield
Impact energy (eV)
Ne on Be
N on Be
D on Be

Figure 9